NANO LETTERS

Letter

pubs.acs.org/NanoLett

# Noncanonical Self-Assembly of Highly Asymmetric Genetically Encoded Polypeptide Amphiphiles into Cylindrical Micelles

Jonathan R. McDaniel,[†,#] Isaac Weitzhandler,[†,#] Sylvain Prevost,[‡] Kevin B. Vargo,[§] Marie-Sousai Appavou,[∥] Daniel A. Hammer,[§] Michael Gradzielski,[‡] and Ashutosh Chilkoti*[,†]

[†]Department of Biomedical Engineering and Research Triangle MRSEC, Duke University, Durham, North Carolina 27708, United States

[‡]Stranski-Laboratorium fur Physikalische und Theoretische Chemie, Institut fur Chemie, Technische Universitat Berlin, 10623, Berlin, Germany

[§]Department of Chemical and Biomolecular Engineering, University of Pennsylvania, Philadelphia, Pennsylvania 19104, United States

[∥]Jülich Centre for Neutron Science (JCNS), Forschungszentrum Jülich GmbH, Outstation at MLZ, Lichtenbergstraße 1, 85747 Garching, Germany

Supporting Information

**ABSTRACT:** Elastin-like polypeptides (ELPs) are a class of biopolymers consisting of the pentameric repeat $(VPG\alpha G)_n$ based on the sequence of mammalian tropoelastin that display a thermally induced soluble-to-insoluble phase transition in aqueous solution. We have discovered a remarkably simple approach to driving the spontaneous self-assembly of high molecular weight ELPs into nanostructures by genetically fusing a short 1.5 kDa $(XG_y)_z$ assembly domain to one end of the ELP. Classical theories of self-assembly based on the geometric mass balance of hydrophilic and hydrophobic block copolymers suggest that these highly asymmetric polypeptides should form spherical micelles. Surprisingly, when sufficiently hydrophobic amino acids (X) are presented in a periodic sequence such as $(FGG)_8$ or $(YG)_8$, these highly asymmetric polypeptides self-assemble into cylindrical micelles whose length can be tuned by the sequence of the morphogenic tag. These nanostructures were characterized by light scattering, tunable resistive pulse sensing, fluorescence spectrophotometry, and thermal turbidimetry, as well as by cryogenic transmission electron microscopy (cryo-TEM) and small-angle neutron scattering (SANS). These short assembly domains provide a facile strategy to control the size, shape, and stability of stimuli responsive polypeptide nanostructures.

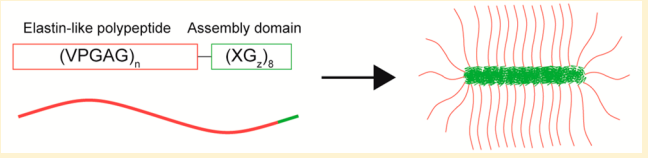


**KEYWORDS:** *Self-assembly, biomaterials, protein polymers, elastin-like polypeptides, cryo-TEM, small-angle neutron scattering*

Self-assembling block copolymer systems have become increasingly popular in recent years due to their suitability for a wide range of applications, including drug delivery,[1−5] sensing,[6] and separations.[7] Block copolymers have been shown to self-assemble into diverse nanoscale morphologies such as wormlike micelles and vesicles,[8] as well as more exotic structures such as multicompartmental micelles,[9] Janus micelles,[10] and asymmetric vesicles.[11] Unfortunately, many morphologically interesting block copolymers are not suitable for biological applications due to their toxicity and low biodegradability. Furthermore, some degree of polydispersity is unavoidable in synthetic polymers, which limits the precision with which their self-assembly can be controlled. In contrast to synthetic polymers, the 20 canonical amino acids are attractive building blocks for polymers due to their lack of toxicity and biodegradability. When synthesized by a genetically encodable methodology they yield monodisperse polymers with precisely controlled stereochemistry. To take advantage of these properties, polypeptides have been incorporated in both copolypeptide (polypeptide−polypeptide) and hybrid (polypeptide−polymer) block copolymers that self-assemble into spherical micelles, wormlike micelles, and vesicles.[12−16]

In recent years, recombinantly synthesized peptide polymers such as elastin-like polypeptides (ELPs) have been increasingly utilized as building blocks for self-assembled systems.[3,4,17−19] ELPs are polymers based on the pentapeptide monomeric repeat $VPG\alpha G$ where the guest residue $\alpha$ can be any amino acid except proline. ELPs exhibit lower critical solution temperature (LCST) phase behavior, whereby below a characteristic temperature the ELP is soluble in solution and above which the ELP phase separates into a polypeptide-rich coacervate. This transition temperature ($T_t$) can be precisely tuned by controlling the chain length of the ELP and the hydrophobicity of the guest residue.[20−22] ELPs have attracted considerable attention due to their nontoxicity, biodegradability, monodispersity, and tunable stimulus-responsive behavior.[20,23] Furthermore, the high degree of control over chain

**Received:** August 21, 2014
**Revised:** September 25, 2014
**Published:** September 30, 2014

   dx.doi.org/10.1021/nl503221p | *Nano Lett.* 2014, 14, 6590−6598

length and behavior afforded by their recombinant design has enabled the use of ELPs for a range of biomedical applications such as drug delivery[24] and tissue engineering.[25] Block copolymers composed of two ELP blocks with sufficiently different hydrophobicities are known to exhibit thermally triggered self-assembly into spherical micelles.[26] Additionally, there are recent reports of an ELP block copolymer self-assembling into vesicles,[27] as well as a protein-ELP fusion self-assembling into wormlike micelles[28] and a peptide-ELP fusion self-assembling into vesicles.[29]

Previous publications from our group describe a remarkably simple approach to building self-assembled ELP nanoparticles that has direct and immediate application in drug delivery. Functionalization of the carboxy-terminus of an ELP with a short $(CGG)_8$ domain provides eight unique sites to which hydrophobic small molecules (e.g., small-molecule chemotherapeutics) can be covalently attached, thereby providing the polymer with sufficiently amphiphilic character to self-assemble into spherical micelles.[4,5,18] The structural similarity of the small molecules previously studied to the aromatic amino acid side chains of tyrosine, phenylalanine, and tryptophan led us to hypothesize that a short $(XGG)_8$ domain (where X = Tyr, Phe, or Trp) could similarly drive self-assembly. The structure of these highly asymmetric amphiphiles follows the motif: (M)SKGPG − $(\alpha GVPG)_n$ − $(XG_y)_8$, where alanine (A) is the guest residue, $n$ is the number of pentameric repeats, X is the identity of the amino acid hydrophobe responsible for driving self-assembly, and $y$ is the number of glycine (G) spacers. The MSKGPG leader is present to enhance expression levels. To investigate this hypothesis, this paper explores the self-assembly behavior of a subset of these sequences by independently modulating these variables in order to better understand how these sequence parameters affect the block copolymer phase transition and morphology. We characterized these polymers by light scattering, fluorescence spectrophotometry, tunable resistive pulse sensing, and thermal turbidimetry. We utilized cryogenic transmission electron microscopy (cryo-TEM) and small-angle neutron scattering (SANS) to obtain a more detailed understanding of the morphology of the self-assembled nanostructures formed by some of these asymmetric amphiphiles.

We find that self-assembly of these peptide-based polymers is governed at the sequence level by both the hydrophobicity of the amino acid X and the number of glycine spacers ($y$). These studies yielded the unexpected observation that, contrary to the canonical theories of polymer self-assembly, some of these block copolymers assemble into cylindrical micelles rather than the expected starlike morphology despite their high degree of asymmetry[30] with a hydrophilic to hydrophobic mass ratio that exceeds 0.95 in some cases. These morphologies suggest that the self-assembly of our peptide-based polymers is not solely driven by hydrophobicity, but also by specific interactions between amino acids that are provided for by their perfectly controlled stereochemistry.

**Results.** *Design of Asymmetric Amphiphiles.* Recombinant methods were used to synthesize a series of asymmetric peptide amphiphiles genetically fused to the carboxy-terminus of an ELP (Table 1, Supporting Information Figure S1).[31] Plasmids coding for the amphiphiles were transformed into *Escherichia coli*, purified after expression by inverse transition cycling,[32,33] lyophilized, and stored at −20 °C for future use. All ELP segments consist of the sequence $(VPGAG)_n$, where the number of pentapeptide repeats "$n$" varies between 40, 80, and 160. Herein, we refer to $(VPGAG)_{40}$ as A40, $(VPGAG)_{80}$ as A80, and $(VPGAG)_{160}$ as A160. The assembly domains consist of the sequence $(XG_y)_8$, where X represents a hydrophobic amino acid[34] and $y$ represents the number of glycine spacers ($y$ = 0, 1, or 2). A C-terminal tyrosine was included to facilitate absorbance-based protein quantification (Supporting Information Figure S1). Following purification, matrix-assisted laser desorption/ionization mass spectrometry (MALDI-MS) was performed on each construct to confirm its molecular weight (Supporting Information Table S1).

**Table 1. Asymmetric Amphiphile Sequences**

| amphiphile | MW g·mol$^{-1}$ | hydrophilic wt % |
|---|---|---|
| A160-$(LGG)_8$ | 63480 | 96.8% |
| A160-$(IGG)_8$ | 63480 | 96.8% |
| A160-$(HGG)_8$ | 63670 | 96.6% |
| A160-$(YGG)_8$ | 63880 | 96.2% |
| A160-$(FGG)_8$ | 63730 | 96.5% |
| A160-$(WGG)_8$ | 64040 | 96.0% |
| A160-$(YG)_8$ | 63400 | 97.0% |
| A160-$Y_8$ | 63000 | 97.6% |
| A160-$(FG)_8$ | 63280 | 97.2% |
| A160-$F_8$ | 62880 | 97.8% |
| A80-$(FGG)_8$ | 33210 | 93.2% |
| A40-$(FGG)_8$ | 17960 | 87.4% |

*Light Scattering.* Each polymer amphiphile was analyzed by dynamic light scattering (DLS) to determine the extent of self-assembly and the hydrodynamic radius of the self-assembled nanoparticle. Amphiphiles with $(XGG)_8$ segments incorporating X = Leu, Ile, His, and Tyr did not self-assemble and remained fully soluble ($R_h$ ∼ 6 nm; Figure 1A, Table 2). Interestingly, peptides incorporating Leu and His at the X position within a $(XGG)_8$ displayed a minor secondary population (an estimated 5−10% of total mass) of self-assembled structures with the remainder unassembled (Supporting Information Figure S5). In contrast, amphiphiles in-corporating Phe (F) or Trp (W) at the X position self-assembled into nanoparticles with hydrodynamic radii ranging from 43 to 81 nm (Table 2).

Surprisingly, we observed that the number of Gly (G) residues within the assembly domain potently controls the self-assembly of these asymmetric amphiphiles. For instance, A160-$(YGG)_8$ displays insufficient amphiphilicity to self-assemble and thus exhibits an $R_h$ of ∼6 nm (Table 2). However, replacing the $(YGG)_8$ domain with a $(YG)_8$ or $Y_8$ domain results in self-assembly into nanoparticles with a $R_h$ of ∼71 and 58 nm, respectively (Table 2). This effect is most likely due to the hydrophilicity of the Gly residues; as the number of glycine residues decreases from 2 to 1 or 0, the overall hydrophobicity of the assembly domain surpasses the threshold necessary to trigger nanoparticle self-assembly. It is clear, however, that not all systems are affected by the number of glycine residues equally; amphiphiles with more hydrophobic assembly domains comprised of Phe self-assemble regardless of the number of Gly spacers (Table 2). In this case, the hydrophobic driving force for self-assembly is strong enough to outweigh the contribution of the Gly residues.

As the ionized form of Tyr ($pK_{aTyr}$ = 10.1) is 10 times more hydrophilic than neutral tyrosine, the A160-$(YG)_8$ construct offered a unique opportunity to confirm that self-assembly is primarily driven by the hydrophobicity of the assembly domain. Upon increasing the pH to 12, the vast majority of the A160-


dx.doi.org/10.1021/nl503221p | Nano Lett. 2014, 14, 6590−6598

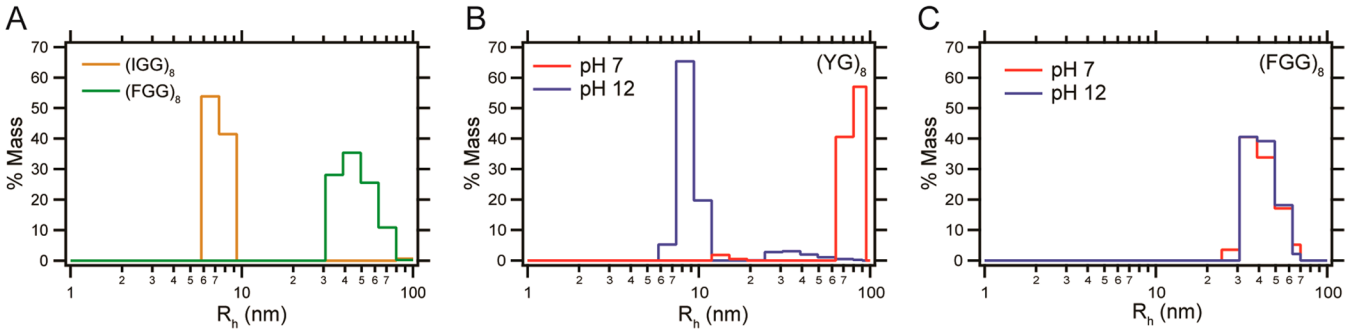


**Figure 1.** Dynamic light scattering results for asymmetric amphiphiles. (A) A160-$(IGG)_8$ does not self-assemble and has a $R_h$ of ∼7 nm, whereas A160-$(FGG)_8$ self-assembles into nanostructures with a $R_h$ of ∼42 nm. (B) A160-$(YG)_8$ self-assembles into nanostructures with a $R_h$ of ∼73 nm that disassemble at pH 12 ($pK_{aTyr}$ = 10.1) because the deprotonation of tyrosine to tyrosinate greatly increases the hydrophilicity of the assembly domain, thereby disrupting the nanoparticle core. (C) A160-$(FGG)_8$ constructs with a $R_h$ of ∼42 nm do not disassemble at high pH because phenylalanine residues do not become charged at high pH.

**Table 2. Amphiphile Characterization by Light Scattering and Tunable Resistive Particle Sizing**

| amphiphile | MW g·mol$^{-1}$ | $N_{agg}$ [a] | $R_g$ [b] (nm) | $R_h$ [c] (nm) | $R$ [d] (nm) | $\rho$ [e] |
|---|---|---|---|---|---|---|
| A160-$(IGG)_8$ | n.d.[f] | n.d.[f] | n.d.[f] | 6.5 ± 0.8 | n.d.[f] | n.d.[f] |
| A160-$(LGG)_8$ | n.d.[f] | n.d.[f] | n.d.[f] | 6.1 ± 0.7 | n.d.[f] | n.d.[f] |
| A160-$(HGG)_8$ | n.d.[f] | n.d.[f] | n.d.[f] | 6.7 ± 0.7 | n.d.[f] | n.d.[f] |
| A160-$(YGG)_8$ | n.d.[f] | n.d.[f] | n.d.[f] | 6.6 ± 0.8 | n.d.[f] | n.d.[f] |
| A160-$(FGG)_8$ | 6.89 × 10$^6$ | 111 | 55.93 | 42.8 ± 9.9 | 53.5 ± 4.8 | 1.31 |
| A160-$(WGG)_8$ | 2.64 × 10$^7$ | 426 | 110.5 | 80.6 ± 35.6 | 76.0 ± 12.1 | 1.37 |
| A160-$(YG)_8$ | 2.47 × 10$^7$ | 399 | 100.0 | 72.7 ± 13.1 | 71.0 ± 8.9 | 1.37 |
| A160-$Y_8$ | 3.36 × 10$^6$ | 53 | 45.0 | 57.85 ± 1.5 | n.d.[g] | 0.78 |
| A160-$(FG)_8$ | 4.68 × 10$^6$ | 76 | 46.1 | 33.0 ± 4.9 | 54.5 ± 5.5 | 1.40 |
| A160-$F_8$ | 3.60 × 10$^7$ | 572 | 124.4 | 91.4 ± 9.7 | 73.0 ± 6.3 | 1.36 |
| A80-$(FGG)_8$ | 9.00 × 10$^6$ | 290 | 47.87 | 35.3 ± 4.3 | 55.5 ± 6.0 | 1.36 |
| A40-$(FGG)_8$ | 8.62 × 10$^6$ | 575 | 44.32 | 30.9 ± 2.6 | 54.5 ± 5.4 | 1.43 |

[a]The aggregation number $N_{agg}$, or the number of polypeptide chains per nanoparticle, was determined by static light scattering [b]$R_g$, radius of gyration, was determined by static light scattering. [c]$R_h$, hydrodynamic radius, was determined by dynamic light scattering. [d]$R$ was determined by tunable resistance pulse sensing. [e]$\rho$ represents the shape factor and is equal to $R_g/R_h$. [f]n.d. indicates no data: static light scattering and TRPS measurements were not performed for nonself-assembling amphiphiles. [g]No data: we were unable to measure the size of A160-$Y_8$ by TRPS.

$(YG)_8$ constructs disassembled into unimers (Figure 1B) because ionizing the tyrosinate residues disrupted the stabilizing hydrophobic cohesion forces in the hydrophobic core. The A160-$(FGG)_8$ constructs, which do not display a $pK_a$ within this range, remained unaffected by the increase in pH (Figure 1C).

For those amphiphiles that self-assembled, static light scattering was used to calculate the aggregation number $N_{agg}$ so as to match Table 2, the number of amphiphile chains per nanoparticle, and the radius of gyration ($R_g$). The nanoparticles displayed aggregation numbers ranging from ∼50 to ∼600 chains per nanoparticle (Table 2) and radii of gyration spanning 45.0 to 124.4 nm (Table 2). The radius of gyration and the hydrodynamic radius were used to calculate the shape factor $\rho = R_g/R_h$, which is characteristic of the morphology of the scatterer, where $\rho$ = 0.775 for solid spheres, $\rho$ = 1 for hollow spheres (vesicles), and $\rho$ = 1.505 for random coils. For cylindrical structures, the relationship between $\rho$ and the elongation $\varepsilon = L/2R$ has been determined as eq 1[35]

$$\rho = \sqrt{\frac{2 + \frac{3}{\varepsilon^2}}{6}}\left[\ln \varepsilon + 0.3675\right] \quad (1)$$

Despite the observed range in nanoparticle size, the shape factor $\rho$ was remarkably consistent between the self-assembling amphiphiles. $\rho$ varied between 1.31 and 1.43, hence indicating a conserved nonspherical morphology and for a rodlike structure according to eq 1 to an axial ratio $\varepsilon$ of 6−8. The one exception, A160-$Y_8$, displayed a $\rho$ value of 0.78, indicating a different morphology. Cryo-TEM and SANS were used to accurately determine the morphologies.

We also investigated the effect of chain length on nanoparticle morphology by examining constructs with an $(FGG)_8$ assembly domain and different lengths of the ELP domain. We observed an increase in the aggregation number from 111 to 290 and 575 as the chain length decreased from 160 to 80 to 40 pentamers, respectively. Surprisingly, only minimal fluctuations in size and morphology were observed with $R_g$ and $R_h$ shrinking slightly and $\rho$ increasing from 1.31 to 1.43.

Tunable resistive pulse sensing, a particle-by-particle analysis technique that relies not on scattering but the physical ability of nanoparticles to pass through a narrow pore was also used as an independent measure of particle size.[36] Radii determined by TRPS were broadly in agreement with the hydrodynamic radii determined by DLS (Table 2, Supporting Information Figure S3).

*LCST Phase Behavior.* We have previously shown that the LCST phase behavior of ELPs is exquisitely sensitive to polypeptide composition,[21] fused proteins[32,37] or chemically conjugated small molecules,[18] ionic strength,[38] and solvent conditions and can be used to drive the self-assembly of gold


dx.doi.org/10.1021/nl503221p | Nano Lett. 2014, 14, 6590−6598

nanoparticles.[39] Thus, it was not surprising to observe that the hydrophobicity of the $(XGG)_8$ assembly domain also affected the LCST phase behavior (Figure 2). In accordance with

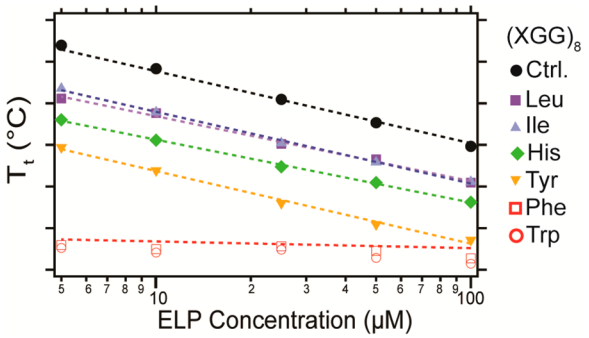


**Figure 2.** LCST phase transition behavior of asymmetric amphiphiles with the sequence A160-$(XGG)_8$. Control denotes an ELP with no assembly domain. $T_t$ of nonself-assembling amphiphiles (control, Leu, Ile, His, and Tyr) display a strong concentration dependence, whereas self-assembling amphiphiles (Phe and Trp) display $T_t$ that are near-independent of concentration.

previous publications characterizing ELPs fused to proteins[37] or chemically conjugated to small molecules,[18] the $T_t$ of the amphiphile decreased as the hydrophobicity of the fused peptide assembly domain increased.[34] We have also shown that the LCST phase transition behavior of unimeric ELPs is concentration-dependent such that a higher concentration of an ELP phase separates at a lower temperature. This inverse relationship between concentration and the transition temperature was observed for all nonself-assembling amphiphiles.[21]

In contrast, the $T_t$ of ELPs that display self-assembly showed virtually no dependence on ELP concentration.[5,40] We hypothesize that this is due to the high and constant local ELP chain concentration within each self-assembled structure, even as the global solution concentration changes. In other words, the ELP chains are entropically trapped once they self-assemble into micelles, and thus the entropic penalty for aggregation is smaller than for the free chains of ELP unimers. The magnitude of this penalty no longer varies significantly with concentration because the structures remain assembled in a similar fashion across a wide range of concentrations. In fact, it is possible to separate the constructs into assembling (X = Phe or Trp) and nonassembling (X = Leu, Ile, His, or Tyr) populations based solely on the thermal turbidimetry profile as a function of concentration (Figure 2).

*Fluorescence Spectrophotometry.* Fluorescence spectrophotometry using pyrene as a probe was performed to sample the hydrophobicity of the inner core of the self-assembled structures and to determine their critical aggregation concentration (CAC).[41] As pyrene is released from the lipophilic core of an assembled nanoparticle to the aqueous environment as a result of nanoparticle disassembly, it experiences a shift in its characteristic fluorescence profile (Figure 3). More specifically, the fluorescent intensity ratio at the 370−373 nm peak to the 381−384 nm peak ($I_1/I_3$) increases sigmoidally as the hydrophilicity of the environment increases. Because nonassembling constructs (e.g., A160-$(YGG)_8$) do not provide a lipophilic environment at any concentration, they exhibit a fluorescence profile that is independent of amphiphile concentration (Figure 3). Additionally, the CAC was used to calculate the free energy of

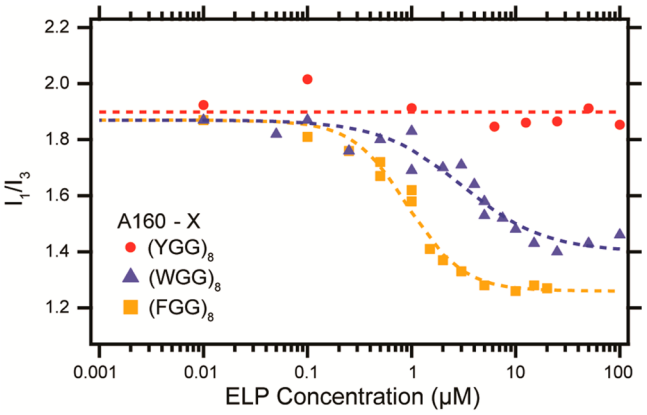


**Figure 3.** Pyrene fluorescence assay of asymmetric amphiphiles. The amphiphile consisting of an A160 ELP and a $(YGG)_8$, assembly domains does not self-assemble and shows no concentration dependence in its $I_1/I_3$ ratio, whereas amphiphiles with $(FGG)_8$ and $(WGG)_8$, assembly domains self-assemble into cylindrical micelles and show a two-state concentration-dependent behavior in their $I_1/I_3$ ratio. The $(FGG)_8$ core is more hydrophobic than the $(WGG)_8$ core, as indicated by its lower final $I_1/I_3$ value.

micellization ($\Delta G_{mic}$) given the relation $\Delta G_{mic} = RT \ln(x_{CAC})$ (where $x_{CAC}$ is the CAC expressed as a mole fraction).

Self-assembling asymmetric amphiphiles display CACs ranging from 0.4 to 13 $\mu$M and free energies of micellization ranging from 37.8 to 46.4 kJ/mol (Table 3). In addition, the

**Table 3. Critical Aggregation Concentration Determined by Pyrene Fluorescence, Core Hydrophobicity (As Measured by Minimum $I_1/I_3$), and Free Enthalpy of Micellization (as Determined from $G_{mic} = RT \ln x_{CAC}$ with $x_{CAC}$ as the CAC Expressed as a Mole Fraction)**

| amphiphile | CAC ($\mu$M) | minimum $I_1/I_3$ | $G_{mic}$ (kJ/mol) |
|---|---|---|---|
| A160-$(FGG)_8$ | 0.9 ± 0.1 | 1.26 | 44.4 |
| A160-$(WGG)_8$ | 3.1 ± 0.4 | 1.41 | 41.4 |
| A160-$(YG)_8$ | 13.0 ± 1.3 | 1.40 | 37.8 |
| A160-$Y_8$ | n.d.[a] | 1.73 | |
| A160-$(FG)_8$ | 2.5 ± 0.2 | 1.31 | 41.9 |
| A160-$F_8$ | 1.3 ± 0.1 | 1.28 | 43.5 |
| A80-$(FGG)_8$ | 0.7 ± 0.1 | 1.20 | 45.1 |
| A40-$(FGG)_8$ | 0.4 ± 0.0 | 1.19 | 46.4 |

[a]n.d. no data: we were unable to measure the CAC of A160-$Y_8$.

minimum $I_1/I_3$ value can be used as a measure of the hydrophobicity of the core. Asymmetric amphiphiles display minima ranging from 1.19 (A40-$(FGG)_8$, most hydrophobic) to 1.41 (A160-$(WGG)_8$, least hydrophobic) (Table 3). Surprisingly, the $(FGG)_8$ domain formed a core that was more hydrophobic than that of $(WGG)_8$ although tryptophan is considered more hydrophobic than phenylalanine.[42] It is possible that the smaller phenylalanine side chains allow higher packing densities or promote enhanced $\pi-\pi$ stacking interactions. We also observed that decreasing the length of the ELP domain from 160 to 40 pentapeptide repeats slightly increases the hydrophobicity and stability of the $(FGG)_8$ core as a function of ELP chain length (Table 3, Supporting Information Figure S6). Despite clear evidence of self-assembled structures by light scattering (Table 2) and cryo-TEM (Figure 4), the pyrene fluorescence data for A160-$Y_8$ indicated that the fluor was in an aqueous environment over a


dx.doi.org/10.1021/nl503221p | Nano Lett. 2014, 14, 6590−6598

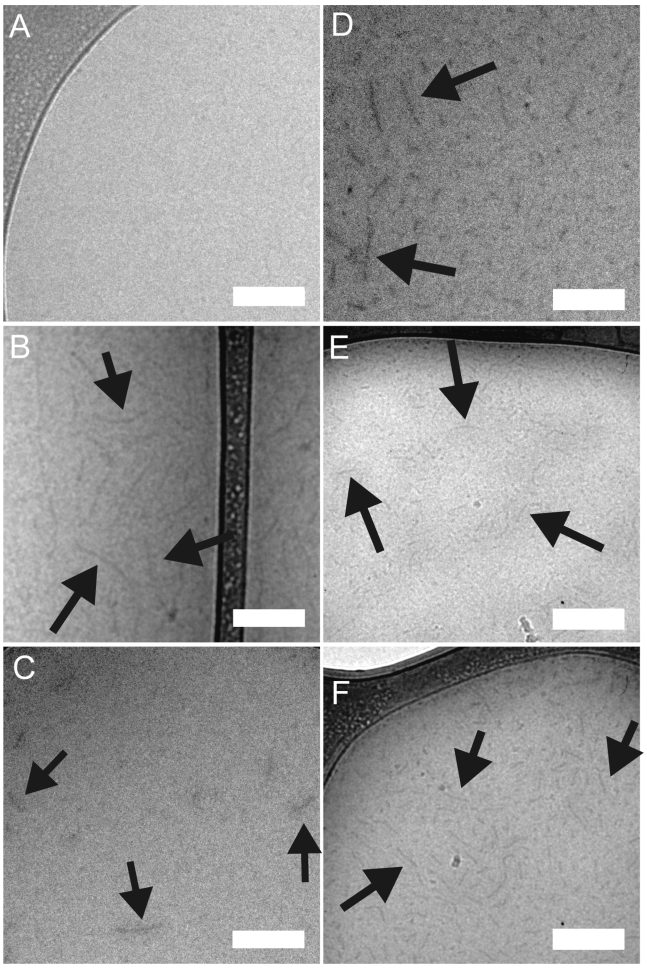


**Figure 4.** Cryo-TEM micrographs of genetically encoded asymmetric amphiphiles. (A–C) A160-$(YGG)_8$, A160-$(YG)_8$, and A160-$Y_8$, respectively. (A) Constructs such as A160-$(YGG)_8$ that do not self-assemble could not be visualized by cryo-TEM because of their high levels of hydration and low densities. (B,C) Changing the assembly domain from $(YG)_8$ (B) to $Y_8$ (C) causes a significant decrease in the length of the cylindrical micelles. (D–F) A160-$(FGG)_8$ (D), A80-$(FGG)_8$ (E), and A40-$(FGG)_8$ (F) self-assemble into cylindrical micelles with similar aspect ratios. Scale bar represents 200 nm.

range of concentrations, thus suggesting a lack of self-assembly. We hypothesize that this artifact may be due to the small size of the core, the low hydrophobicity of the core, or a combination of these two factors.

*Cryogenic Transmission Electron Microscopy.* Cryo-TEM experiments were performed to directly visualize the self-assembled structures in their near-native hydrated state. However, due to their relatively low electron density, polypeptide amphiphiles are challenging to image by cryo-TEM as they exhibit lower contrast than many synthetic polymer amphiphiles. Samples were imaged at a low voltage (80 keV) to increase the contrast between the buffer and the polypeptide chains. Although the hydrophobic cores have sufficient electron density to be clearly visualized by cryo-TEM under these conditions, we were unable to visualize the hydrated ELP corona in self-assembled structures or single ELP chains (unimers) due to their low electron density and high degree of solvation.

In contrast to conjugation-driven assembly, which only yields spherical micelles,[18] these asymmetric amphiphiles spontaneously assemble into cylindrical micelles upon achieving sufficient hydrophobicity in the core (Figure 4A–F). For instance, the A160 amphiphile with a terminal $(YGG)_8$ domain showed no self-assembly, but as the glycine fraction in the assembly domain was reduced with $(YG)_8$ and $Y_8$ assembly domains, amphiphiles spontaneously self-assembled into cylindrical micelles (Figure 4B–C). We found that the Gly content of the self-assembly domain controls the length of the micelles and hence their aspect ratio. Although the radii remained approximately 11.5 nm for both the A160-$(YG)_8$ and A160-$Y_8$ constructs, the length decreased from 119 nm for the $(YG)_8$ construct to 60 nm for the $Y_8$ construct, resulting in a decreased aspect ratio (Table 4).

**Table 4. Size Parameters of Cylindrical Micelles As Measured by cryo-TEM**

| amphiphile | length (nm)[a] | radius (nm)[a] | apparent aspect ratio ($L/R$)[b] |
|---|---|---|---|
| A40-$(FGG)_8$ | 56.6 ± 26.0 | 6.5 ± 1.5 | 8.7 ± 1.1 |
| A80-$(FGG)_8$ | 63.5 ± 25.4 | 6.5 ± 1.5 | 9.8 ± 1.1 |
| A160-$(FGG)_8$ | 110.2 ± 34.0 | 10.0 ± 1.7 | 11.0 ± 1.1 |
| A160-$(YG)_8$ | 118.6 ± 32.5 | 11.8 ± 1.9 | 10.1 ± 3.2 |
| A160-$Y_8$ | 59.7 ± 11.3 | 11.3 ± 3.5 | 5.3 ± 0.6 |

[a]Data are reported as mean ± standard deviation with a minimum of 25 measurements. [b]This apparent aspect ratio is defined only by the portion of the assembly that is visible by cryo-TEM and as such differs from the true aspect ratio determined by scattering.

The cryo-TEM results were also consistent with results from light scattering. This change in aspect ratio is consistent with the $\rho$ values of 1.37 and 0.78 observed for A160-$(YG)_8$ and A160-$Y_8$, respectively (Table 2). The $\rho$ value of 0.78 for A160-$(YG)_8$ seemingly indicates a spherical morphology; however, cryo-TEM reveals that it is in fact a cylindrical morphology with a low aspect ratio. Whereas the composition of the assembly domain played a role in controlling the aspect ratio of the nanoparticles, the length of the ELP domain (160, 80, and 40 pentapeptides) attached to the $(FGG)_8$ assembly domain only resulted in minor differences in the aspect ratio (Figure 4D–F, Table 4).

*Small-Angle Neutron Scattering (SANS).* To gain deeper insight into the nanometer scale structure of these self-assembled constructs, SANS spectra of A160-$(FGG)_8$ and A160-$(YG)_8$ were acquired at concentrations ranging from 0.3 to 3 wt % in $D_2O$ (Figure 5). The SANS data span a $q$-range of 0.02–4 $nm^{-1}$ ($q$: magnitude of the wave vector), which roughly translates to 1.5–300 nm in real space.

The spectra for both amphiphiles are very similar, and a number of structural features can be deduced directly from the spectra. The scattering intensity for both amphiphiles follows a $q^{-2}$ power law at mid to high $q$, which is typical for polymer chains. At $q \approx 0.15$ $nm^{-1}$ the intensity increases abruptly, corresponding to a cross-sectional radius of $3.83 \cdot q^{-1}$ for cylinders (26 nm) and then plateaus at lower $q$, hence indicating that the largest scattering dimension is approximately 150 nm. VSANS (very small-angle neutron scattering) experiments were performed at lower $q$ to confirm this size limit (Supporting Information Figure S7). The concentration series data reveal strong repulsive interactions visible as a structure factor correlation peak. As they likely arise from excluded volume effects and given the low volume fraction of


dx.doi.org/10.1021/nl503221p | Nano Lett. 2014, 14, 6590–6598

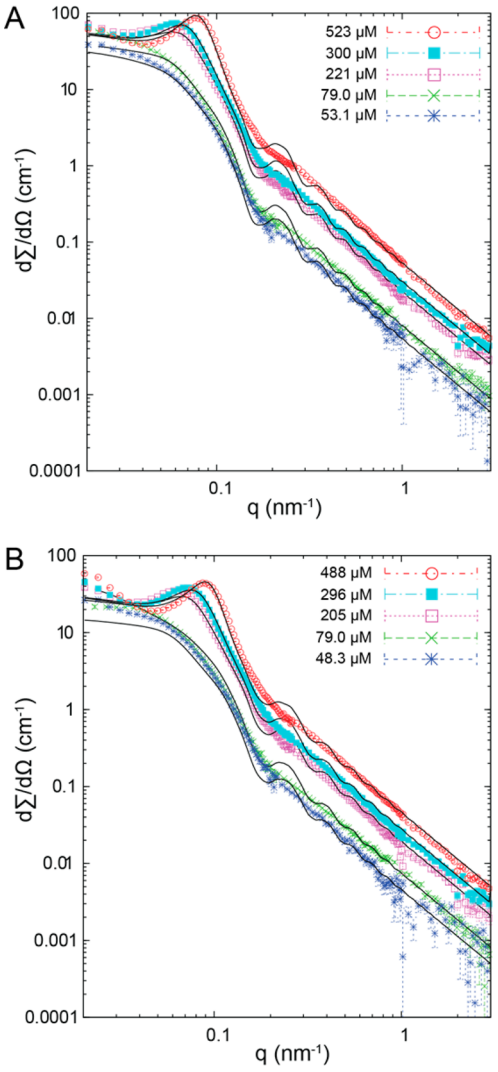


**Figure 5.** SANS spectra and analytical model fits (solid lines) for A160-$(FGG)_8$ (A) and A160-$(YG)_8$ (B). The $q^{-2}$ slope in the mid to high $q$ region is characteristic of the polymer chains in the hydrophilic part of the nanostructures. The structure factor peak at low $q$ is caused by repulsive interactions between structures.

amphiphiles, this can only be explained by a high degree of solvation of the nanostructures.

To obtain more reliable values for the size parameters of these micelles, next we analytically modeled the SANS spectra. On the basis of cryo-TEM data, we chose a model of isotropically oriented homogeneous cylindrical micelles that also incorporated scattering from individual polypeptide chains at smaller length scales[43−45] (see Supporting Information). To obtain a robust set of output parameters, we simultaneously fitted all spectra from a given amphiphile with the same parameter set, thus covering a wide concentration range. For A160-$(FGG)_8$ and A160-$(YG)_8$ the cylinder lengths obtained from the model are 174 and 164 nm and the radii are 24 and 21 nm, respectively, corresponding to an axial ratio $\varepsilon$ of ∼4, which is in good agreement with the light scattering data. The $R_g$ of the individual polymer chains (the hydrophilic ELP brush) is 11 nm and the hydration of the micelles (the volume fraction of the nanostructure occupied by water) is 0.94. These dimensions are slightly larger than those observed by cryo-TEM. However, in cryo-TEM it is possible that many of the cylindrical micelles are tilted within the vitreous ice layer, leading to a lower observed length. It is also possible that the outer region of the core is too highly solvated to be observed by cryo-TEM, thus explaining the larger radius observed by SANS.

**Discussion.** We have observed that amphiphilic block copolymers comprised of a water-soluble polypeptide and an extremely short hydrophobic peptide self-assemble into cylindrical micelles. This observation is highly surprising and contrary to accepted theories of self-assembly of synthetic block copolymers because their extremely high hydrophilic weight fraction would predict either a lack of self-assembly or assembly into star-like micelles. We also observed that self-assembly is highly sensitive to the hydrophobicity of the assembly domain: less hydrophobic residues such as Leu and Ile do not drive self-assembly, whereas the more hydrophobic Tyr, Phe, and Trp residues spontaneously form nanoparticles. Self-assembly is also sensitive to the number of glycine residues between the hydrophobic residues. For instance, the $(YGG)_8$ domain was not sufficiently hydrophobic to drive self-assembly of A160 ELP, whereas both the $(YG)_8$ and $Y_8$ domains drove self-assembly into cylindrical micelles.

Among the self-assembling constructs, the $R_g$ and $R_h$ determined by light scattering varied substantially (from 46.1 to 124.4 nm and from 33.0 to 91.4 nm, respectively), while the shape factor $\rho$ ($R_g/R_h$) remained remarkably constant (varying only between 1.31 and 1.43) for all but one amphiphile. Cryo-TEM revealed that all constructs other than A160-$Y_8$ self-assembled into similar cylindrical morphologies, and A160-$Y_8$ self-assembled into cylindrical micelles with a significantly lower aspect ratio. In addition to cryo-TEM, SANS provided a complementary ensemble measurement that confirmed the cylindrical morphology with core radii of 21−23 nm and a length of ∼170 nm.

All amphiphiles retained the stimulus-responsiveness of the parent ELP chain with nonself-assembling constructs exhibiting a significant concentration dependence in their $T_t$, while the self-assembling constructs displayed little to no concentration dependence in their $T_t$. Fluorescence spectroscopy using pyrene as a probe revealed that despite their similar morphologies, the cylindrical micelles formed cores with varying levels of hydrophobicity (as measured by the characteristic fluorescence behavior of pyrene) and displayed a range of CACs from 0.4 to 13.0 $\mu$M. These low CACs correspond to relatively high values for the Gibbs free energy of micellization of 40−45 kJ/mol, which indicate the strongly amphiphilic character of these compounds.

Our most unexpected finding is that asymmetric amphiphiles with hydrophilic fractions as high as 97% self-assemble into cylindrical micelles rather than spherical micelles. Synthetic block copolymers canonically form spherical micelles when the hydrophilic weight fraction exceeds 60%, cylindrical micelles are favored between 45% and 55%, and vesicles are constrained to the region between 25% and 45%.[30,46] The free energy of self-assembly and thus the morphology are determined primarily by the stretching of the core-forming block, the repulsion between the corona blocks, and the interfacial tension between the core and the solvent.[47] Surprisingly, within the sequence space sampled here the hydrophilic fraction does not seem to play a significant role in determining the morphology, as phenylalanine-based constructs with hydrophilic fractions of 97% (chain length $n$ = 160), 94% ($n$ = 80), and 88% ($n$ = 40) all assembled into similar cylindrical nanostructures as seen by cryo-TEM and light scattering. However, the hydrophilic


dx.doi.org/10.1021/nl503221p | Nano Lett. 2014, 14, 6590−6598

fraction significantly influenced the aggregation number with higher hydrophilic fractions leading to fewer polypeptide chains per nanoparticle.

The self-assembly of these asymmetric amphiphiles also raises more fundamental questions about how the self-assembly of polypeptide chains differs from that of synthetic polymers. The nature of the hydrophobic interactions in the core of asymmetric amphiphiles is not yet well understood. Given the aromatic groups present in Tyr, Phe, and Trp side-chains, we believe that $\pi-\pi$ stacking of aromatic groups may play an important and as yet unexplored role in amphiphile self-assembly. The fact that the core diameter observed by SANS is larger than the stretched length of the hydrophobic assembly domain also indicates that part of the hydrophilic ELP chain may be collapsed onto the hydrophobic core. The slight increase in the hydrophobicity of the core as the ELP block is shortened from 160 to 80 and 40 with an assembly domain of $(FGG)_8$ (as measured by pyrene $I_1/I_3$, Table 3) is consistent with this hypothesis, as it indicates that the hydrophobic region may consist not only of the $(FGG)_8$ domain but also of a portion of the ELP domain. We anticipate addressing these questions in future studies.

In addition to their interesting material characteristics, this class of self-assembling amphiphiles should be useful for a number of biomedical applications. For instance, promoting self-assembly via a genetically encoded peptide instead of a chemically conjugated hydrophobe could allow for hydrophilic drugs to be repurposed into therapeutic nanoparticles. While water-soluble chemotherapeutics display improved pharmacokinetics and biodistribution relative to their hydrophobic counterparts, they are still plagued by rapid deactivation in serum,[48,49] clearance from circulation,[50] and nonspecific absorption into healthy tissues.[51] In the case of hydrophobic therapeutics, these issues are typically ameliorated by the sequestration of the drug into a protected nanoparticle core.[52−57] The design of triblock peptide polymers with an ELP segment, followed by a drug attachment domain and an assembly domain, could result in self-assembly into stable nanostructures despite the conjugation of a hydrophilic therapeutic within the core.

**Materials and Methods.** *Materials.* Restriction enzymes and T4 DNA ligase were purchased from New England Biolabs (Ipswich, MA). All custom oligonucleotides were synthesized by Integrated DNA Technologies Inc. (Coralville, IA). The DNA miniprep and gel purification kits were purchased from Qiagen Inc. (Germantown, MD). EB5$\alpha$ and BL21 (DE3) *Escherichia coli* cells were purchased from Edge BioSystems (Gaithersburg, MD). All *Escherichia coli* cultures were grown in TBDry media purchased from MO BIO Laboratories, Inc. (Carlsbad, CA). Kanamycin was purchased from CalBioChem (San Diego, CA).

*Synthesis of Asymmetric Polypeptides.* The highly asymmetric amphiphiles were synthesized from synthetic oligomers using plasmid reconstruction recursive directional ligation.[31] The asymmetric amphiphiles described in this chapter are of the form SKGPG-$(AGVPG)_n$-$(XG_y)_8$-Y, where the polypeptide length $n$ (40, 80, or 160), the number of glycine spacers $y$ (0, 1, or 2), and the identity of the hydrophobic residue X are systematically varied (Table 1, Supporting Information Figure S1).

*Expression and Purification of Asymmetric Amphiphiles.* Each construct was expressed using a previously published hyperexpression protocol, which relies on the leakiness of the T7 promoter.[58] Fifty milliliter cultures were grown overnight and used to inoculate 1 L flasks of TBDry supplemented with 45 $\mu$g/mL kanamycin. The flasks were then incubated at 37 °C for 24 h and 190 rpm. Each construct was purified using a modified Inverse Transition Cycling (ITC) protocol,[32,33] where the solution was never heated above room temperature. Briefly, the cell suspension was centrifuged at 3000 rpm for 10 min at 4 °C, the cell pellet resuspended in PBS, and then lysed by sonication on ice for 3 min (10 s on, 40 s off) (Masonix S-4000; Farmingdale, NY). Polyethylenimine 0.7% w/v was added to the lysate to precipitate nucleic acid contaminants. The supernatant was then subjected to multiple rounds of ITC as follows. The solution was kept on ice, and 3 M NaCl was added to isothermally trigger the phase transition of the ELP. The coacervate was then centrifuged for 10 min at 14 000$g$ and 20 °C, the supernatant was decanted and discarded, and the pellet was resuspended in phosphate buffer. This suspension was cooled to 4 °C, and then centrifuged for 10 min at 14 000 and 4 °C to remove any insoluble contaminants.

*Thermal Turbidimetry.* Turbidity profiles were obtained for each of the constructs by recording the optical density as a function of temperature (1 °C/min ramp) on a temperature controlled UV−vis spectrophotometer (Cary 300 Bio; Varian Instruments; Palo Alto, CA). The $T_t$ was defined as the inflection point of the turbidity profile. Samples were measured in PBS at five different solution concentrations between 1−100 $\mu$M.

*Light Scattering.* Dynamic light scattering was used to determine the hydrodynamic radius ($R_h$) of the various constructs at 25 °C and 25 $\mu$M amphiphile concentration using a Dynapro plate reader (Wyatt Technology; Santa Barbara, CA), following filtration through 0.22 $\mu$m Millex-GV filters (Millipore; Billerica, MA). The data was analyzed with a regularization fit for Raleigh spheres. Additional dynamic and static light scattering measurements were performed using an ALV/CGS-3 goniometer system (Germany). Samples for the ALV/CGS-3 goniometer system were prepared in PBS at 25 $\mu$M and filtered through 0.22 $\mu$m Millex-GV filters into a 10 mm disposable borosilicate glass tube (Fischer). Measurements were obtained at 25 °C for angles between 30−150° at 5° increments with each angle consisting of 3 runs for 10 s. Results were analyzed by partial Zimm plot analysis using ALV/Dynamic and Static FIT and PLOT software.

*Tunable Resistive Pulse Sensing.* Lyophilized samples were resuspended in PBS to a concentration of 50 $\mu$M and filtered through 0.22 $\mu$m Millex-GV filters. Forty microliters of the sample was loaded onto a qNano (Izon; Christchurch, New Zealand) instrument equipped with 50−150 nm pores (A160-$(FGG)_8$, A160-$(FG)_8$, A80-$(FGG)_8$, and A40-$(FGG)_8$) or 100−300 nm pores (A160-$(YG)_8$, A160-$F_8$, and A160-$(WGG)_8$). Samples were measured for at least 30 s and a minimum of 500 blockade events were recorded per sample. Samples were calibrated against known standards (Izon) for the same stretch and voltage.

*Fluorescence Spectroscopy.* An assay to determine the critical aggregation concentration (CAC) using pyrene as a probe was performed using a Cary Eclipse spectrophotometer equipped with a Xenon flash lamp (Varian Instruments; Palo Alto, CA). One microliter of a stock solution of 12 mM pyrene (Fluka/Sigma-Aldrich; St. Louis, MO) in ethanol was diluted into 20 mL of PBS. Both the stock solution and diluted pyrene solution in PBS were sonicated for 10 min prior to use. One to five milligrams of lyophilized ELP was added to this solution,


dx.doi.org/10.1021/nl503221p | Nano Lett. 2014, 14, 6590−6598

which was then used to create a dilution series for that ELP. Each sample was placed in a reduced volume cuvette and scanned (Ex, 334; Em, 360−380; Ex slit 10 nm; Em slit 2.5 nm). Pyrene fluorescence displays four peaks; the intensity of the first ($I_1$, 370−373 nm) and third peak ($I_3$, 381−384 nm) were recorded. The ratio $I_1/I_3$ was plotted as a function of amphiphile concentration, and the CAC was defined as the inflection point of the sigmoid of best fit.

*Cryogenic Transmission Electron Microscopy.* Cryo-TEM experiments were performed at Duke University's Shared Materials Instrumentation Facility (Durham, NC) and at the University of Pennsylvania in the Penn Regional Nanotechnology Facility (Philadelphia, PA). At Duke University, lacey holey carbon grids (Ted Pella, Redding, CA) were glow discharged in a PELCO EasiGlow Cleaning System (Ted Pella, Redding, CA). A 3 μL drop (200 μM ELP concentration) was deposited onto the grid, blotted for 3 s with an offset of −3 mm, and vitrified in liquid ethane using the Vitrobot Mark III (FEI, Eindhoven, Netherlands). Prior to vitrification, the sample chamber was maintained at 22 °C and 100% relative humidity to prevent sample evaporation. Grids were transferred to a Gatan 626 cryoholder (Gatan, Pleasanton, CA) and imaged with an FEI Tecnai $G^2$ Twin TEM (FEI, Eindhoven, Netherlands), operating at 80 keV.

At the University of Pennsylvania, lacey Formvar/carbon grids (Ted Pella) were washed in chloroform to remove the Formvar template and carbon coated with a Quorum Q150T ES carbon coater (Quorum Technologies, United Kingdom). Grids were cleaned with hydrogen/oxygen plasma for 15 s using the Solarus Advanced Plasma System 950 (Gatan, Pleasanton, CA). A 2 μL drop (200 μM ELP concentration) was deposited onto the grid and added to a Gatan Cp3 cryoplunger (Gatan, Pleasanton, CA). The samples were blotted by hand and plunged into liquid ethane. Grids were transferred to a Gatan CT3500TR cryoholder (Gatan, Pleasanton, CA) and immediately inserted into a JEOL 2010 TEM (JEOL, Tokyo, Japan) operating at 80 keV.

*Small-Angle Neutron Scattering (SANS).* SANS experiments were conducted at the Jülich Center for Neutron Science at MLZ in Munich, Germany, in duplicate (two independent samples measured on two similar instruments: KWS-1 and KWS-2).[59] Samples were poured into quartz cuvettes and acquisitions were performed at room temperature (observed temperature: 21.5 ± 1.5 °C). $D_2O$ was used as a solvent to increase the contrast (difference in scattering length densities, ΔSLD) and decrease the incoherent background mainly caused by hydrogen. Three configurations were used at a fixed wavelength of 0.46 nm (with full width at half-maximum of 10% on KWS-1 and 20% on KWS-2), changing the sample-to-detector distance (1, 5, and 20 m). Data were reduced in the small-angle approximation using the BerSANS software program,[60] correcting measured intensities for the transmission, dead-time, detector background (with $B_4C$ as a neutron absorber at the sample position), sample background (either the empty cuvette or the solvent) and light water (1 mm neutron pathway) for the flat field. The absolute scale was obtained from a tabulated value of a 1.5 mm sheet of Plexiglas. Very small-angle neutron scattering (VSANS) data were measured on KWS-3 at MLZ, at a wavelength of 1.2 nm and a sample-to-detector distance of 9.5 m with a beam aperture of 2 × 2 $mm^2$, the detector being at the focal point of the beam. Samples were in the same quartz QX cuvettes as for SANS. The data reduction was performed using the facility's software (QtiKWS). Absolute scale was obtained from the direct beam measurement. The scattering from a cuvette filled with $D_2O$ (2 mm pathway) was subtracted. The SLDs were calculated with values from Jacrot,[61] assuming that all exchangeable protons were replaced by deuterons. The solvent ($D_2O$) SLD is 6.36 × $10^{-4}$ $nm^{-2}$.

## ■ ASSOCIATED CONTENT

### Supporting Information

Gene sequences, agarose gel of digested gene library, MALDI-MS, tunable resistive pulse sensing, additional thermal turbidimetry and pyrene analysis, SANS model details, and additional SANS fitting. This material is available free of charge via the Internet at http://pubs.acs.org.

## ■ AUTHOR INFORMATION

### Corresponding Author

*E-mail: chilkoti@duke.edu.

### Present Address

(J.R.M.) Department of Chemical Engineering, Institute for Molecular and Cellular Biology, University of Texas at Austin, Austin, TX 78712-1062.

### Author Contributions

#J.R.M. and I.W. contributed equally.

All authors have given approval to the final version of the manuscript.

### Notes

The authors declare no competing financial interest.

## ■ ACKNOWLEDGMENTS

This work was partially supported by a grant from the NIH (R01 GM-61232) to A.C. and by the NSF through the Research Triangle MRSEC (NSF-DMR-11-21107). I.W. acknowledges support in the form of a National Science Foundation Graduate Research Fellowship (NSF-DGE-1106401). The Jülich Center for Neutron Science (JCNS) is thanked for granting beamtime. S.P. acknowledges the financial support provided by JCNS to perform the neutron scattering measurements at the Heinz Maier-Leibnitz Zentrum (MLZ), Garching, Germany as well as technical assistance from Dr. Vitaliy Pipich for the VSANS experiments. D.A.H. acknowledges financial support from NSF DMR-1309556 and NSF DMR-1120901.

## ■ ABBREVIATIONS

ELP, elastin-like polypeptide; DLS, dynamic light scattering; SLS, static light scattering; CAC, critical aggregation concentration; cryo-TEM, cryogenic transmission electron microscopy; SANS, small-angle neutron scattering

## ■ REFERENCES

(1) Kakizawa, Y.; Harada, A.; Kataoka, K. *Biomacromolecules* **2001**, *2*, 491−7.

(2) Kataoka, K.; Harada, A.; Nagasaki, Y. *Adv. Drug Delivery Rev.* **2001**, *47*, 113−31.

(3) Macewan, S. R.; Chilkoti, A. *Nano Lett.* **2012**, *12*, 3322−8.

(4) MacKay, J. A.; Chen, M.; McDaniel, J. R.; Liu, W.; Simnick, A. J.; Chilkoti, A. *Nat. Mater.* **2009**, *8*, 993−9.

(5) McDaniel, J. R.; Macewan, S. R.; Dewhirst, M.; Chilkoti, A. *J. Controlled Release* **2012**, *159*, 362−7.

(6) Senaratne, W.; Andruzzi, L.; Ober, C. K. *Biomacromolecules* **2005**, *6*, 2427−48.

(7) Najer, A.; Wu, D.; Vasquez, D.; Palivan, C. G.; Meier, W. *Nanomedicine* **2013**, *8*, 425−47.
(8) Jenekhe, S. A.; Chen, X. L. *Science* **1998**, *279*, 1903−1907.
(9) Li, Z.; Kesselman, E.; Talmon, Y.; Hillmyer, M. A.; Lodge, T. P. *Science* **2004**, *306*, 98−101.
(10) Erhardt, R.; Zhang, M.; Boker, A.; Zettl, H.; Abetz, C.; Frederik, P.; Krausch, G.; Abetz, V.; Muller, A. H. *J. Am. Chem. Soc.* **2003**, *125*, 3260−7.
(11) Stoenescu, R.; Graff, A.; Meier, W. *Macromol. Biosci.* **2004**, *4*, 930−5.
(12) Carlsen, A.; Lecommandoux, S. *Curr. Opin. Colloid Interface Sci.* **2009**, *14*, 329−339.
(13) Holowka, E. P.; Pochan, D. J.; Deming, T. J. *J. Am. Chem. Soc.* **2005**, *127*, 12423−12428.
(14) Holowka, E. P.; Sun, V. Z.; Kamei, D. T.; Deming, T. J. *Nat. Mater.* **2007**, *6*, 52−57.
(15) Constancis, A.; Meyrueix, R.; Bryson, N.; Huille, S.; Grosselin, J.-M.; Gulik-Krzywicki, T.; Soula, G. *J. Colloid Interface Sci.* **1999**, *217*, 357−368.
(16) Sun, J.; Shi, Q.; Chen, X.; Guo, J.; Jing, X. *Macromol. Chem. Phys.* **2008**, *209*, 1129−1136.
(17) Ghoorchian, A.; Cole, J. T.; Holland, N. B. *Macromolecules* **2010**, *43*, 4340−4345.
(18) McDaniel, J. R.; Bhattacharyya, J.; Vargo, K. B.; Hassouneh, W.; Hammer, D. A.; Chilkoti, A. *Angew. Chem., Int. Ed.* **2013**, *52*, 1683−7.
(19) Janib, S. M.; Pastuszka, M. F.; Aluri, S.; Folchman-Wagner, Z.; Hsueh, P. Y.; Shi, P.; Lin, Y. A.; Cui, H.; MacKay, J. A. *Polym. Chem.* **2014**, *5*, 1614−1625.
(20) Meyer, D. E.; Chilkoti, A. *Biomacromolecules* **2004**, *5*, 846−51.
(21) McDaniel, J. R.; Radford, D. C.; Chilkoti, A. *Biomacromolecules* **2013**, *14*, 2866−72.
(22) McDaniel, J. R.; Macewan, S. R.; Li, X.; Radford, D. C.; Landon, C. D.; Dewhirst, M.; Chilkoti, A. *Nano Lett.* **2014**, DOI: 10.1021/nl5009376.
(23) Urry, D. W.; Parker, T. M.; Reid, M. C.; Gowda, D. C. *J. Bioact. Compat. Polym.* **1991**, *6*, 263−282.
(24) Mastria, E.; Chilkoti, A. *MRS Bull.* **2014**, *39*, 35−43.
(25) Nettles, D. L.; Chilkoti, A.; Setton, L. A. *Adv. Drug Delivery Rev.* **2010**, *62*, 1479−85.
(26) Wright, E. R.; Conticello, V. P. *Adv. Drug Delivery Rev.* **2002**, *54*, 1057−1073.
(27) Martin, L.; Castro, E.; Ribeiro, A.; Alonso, M.; Rodriguez-Cabello, J. C. *Biomacromolecules* **2012**, *13*, 293−298.
(28) Aluri, S. R.; Shi, P.; Gustafson, J. A.; Wang, W.; Lin, Y. A.; Cui, H.; Liu, S.; Conti, P. S.; Li, Z.; Hu, P.; Epstein, A. L.; Mackay, J. A. *ACS Nano* **2014**, *8*, 2064−2076.
(29) Pastuszka, M. K.; Wang, X.; Lock, L. L.; Janib, S. M.; Cui, H.; DeLeve, L. D.; MacKay, J. A. *J. Controlled Release* **2014**, *191*, 15−23.
(30) Srinivas, G.; Discher, D. E.; Klein, M. L. *Nat. Mater.* **2004**, *3*, 638−44.
(31) McDaniel, J. R.; Mackay, J. A.; Quiroz, F. G.; Chilkoti, A. *Biomacromolecules* **2010**, *11*, 944−52.
(32) Meyer, D. E.; Chilkoti, A. *Nat. Biotechnol.* **1999**, *17*, 1112−5.
(33) Trabbic-Carlson, K.; Liu, L.; Kim, B.; Chilkoti, A. *Protein Sci.* **2004**, *13*, 3274−84.
(34) Urry, D. W. *Chem. Phys. Lett.* **2004**, *399*, 177−183.
(35) Ortega, A.; García de la Torre, J. *J. Chem. Phys.* **2003**, *119*, 9914−9919.
(36) Kozak, D.; Anderson, W.; Vogel, R.; Trau, M. *Nano Today* **2011**, *6*, 531−545.
(37) Hassouneh, W.; Fischer, K.; MacEwan, S. R.; Branscheid, R.; Fu, C. L.; Liu, R.; Schmidt, M.; Chilkoti, A. *Biomacromolecules* **2012**, *13*, 1598−605.
(38) Cho, Y.; Zhang, Y.; Christensen, T.; Sagle, L. B.; Chilkoti, A.; Cremer, P. S. *J. Phys. Chem. B* **2008**, *112*, 13765−71.
(39) Nath, N.; Chilkoti, A. *J. Am. Chem. Soc.* **2001**, *123*, 8197−202.
(40) Weller, D.; McDaniel, J. R.; Fischer, K.; Chilkoti, A.; Schmidt, M. *Macromolecules* **2013**, *46*, 4966−4971.
(41) Kalyanasundaram, K.; Thomas, J. K. *J. Am. Chem. Soc.* **1977**, *99*, 2039−2044.
(42) Urry, D. W.; Gowda, D. C.; Parker, T. M.; Luan, C. H.; Reid, M. C.; Harris, C. M.; Pattanaik, A.; Harris, R. D. *Biopolymers* **1992**, *32*, 1243−50.
(43) Fournet, A. G. a. G. *J. Polym. Sci.* **1956**, *19*, 594−594.
(44) Debye, P. *J. Phys. Colloid Chem.* **1947**, *51*, 18−32.
(45) Wertheim, M. S. *Phys. Rev. Lett.* **1963**, *10*, 321−323.
(46) Vargo, K. B.; Parthasarathy, R.; Hammer, D. A. *Proc. Natl. Acad. Sci. U.S.A.* **2012**, *109*, 11657−62.
(47) Mai, Y.; Eisenberg, A. *Chem. Soc. Rev.* **2012**, *41*, 5969−5985.
(48) Abbruzzese, J. L.; Grunewald, R.; Weeks, E. A.; Gravel, D.; Adams, T.; Nowak, B.; Mineishi, S.; Tarassoff, P.; Satterlee, W.; Raber, M. N.; Plunkett, W. *J. Clin. Oncol.* **1991**, *9*, 491−8.
(49) Burke, T. G.; Mi, Z. *Anal. Biochem.* **1993**, *212*, 285−7.
(50) Guichard, S.; Montazeri, A.; Chatelut, E.; Hennebelle, I.; Bugat, R.; Canal, P. *Clin. Cancer. Res.* **2001**, *7*, 3222−8.
(51) Abratt, R. P.; Bezwoda, W. R.; Falkson, G.; Goedhals, L.; Hacking, D.; Rugg, T. A. *J. Clin. Oncol.* **1994**, *12*, 1535−40.
(52) Veronese, F. M.; Schiavon, O.; Pasut, G.; Mendichi, R.; Andersson, L.; Tsirk, A.; Ford, J.; Wu, G.; Kneller, S.; Davies, J.; Duncan, R. *Bioconjugate Chem.* **2005**, *16*, 775−84.
(53) Lee, C. C.; Gillies, E. R.; Fox, M. E.; Guillaudeu, S. J.; Frechet, J. M.; Dy, E. E.; Szoka, F. C. *Proc. Natl. Acad. Sci. U.S.A.* **2006**, *103*, 16649−54.
(54) Cheng, J.; Khin, K. T.; Jensen, G. S.; Liu, A.; Davis, M. E. *Bioconjugate Chem.* **2003**, *14*, 1007−17.
(55) Otsuka, H.; Nagasaki, Y.; Kataoka, K. *Adv. Drug Delivery Rev.* **2003**, *55*, 403−19.
(56) Kojima, C.; Kono, K.; Maruyama, K.; Takagishi, T. *Bioconjugate Chem.* **2000**, *11*, 910−7.
(57) Meng, F.; Zhong, Z.; Feijen, J. *Biomacromolecules* **2009**, *10*, 197−209.
(58) Guda, C.; Zhang, X.; Mcpherson, D. T.; Xu, J.; Cherry, J. H.; Urry, D. W.; Daniell, H. *Biotechnol. Lett.* **1995**, *17*, 745−750.
(59) Radulescu, A.; Pipich, V.; Frielinghaus, H.; Appavou, M.-S. KWS-2, the high intensity/wide Q-range small-angle neutron diffractometer for soft-matter and biology at FRM II. *J. Phys.: Conf. Ser.* **2012**, 012026.
(60) Keiderling, U. *Appl. Phys. A.* **2002**, *74*, s1455−s1457.
(61) Jacrot, B. *Rep. Prog. Phys.* **1976**, *39*, 911−953.